Powder Technology 453 (2025) 120605

Contents lists available at ScienceDirect

Powder Technology

journal homepage: www.journals.elsevier.com/powder-technology

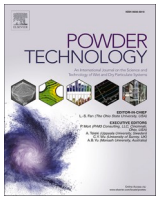

# Dynamic adhesion measurement of powders using the drop testing method: Defining a window of operation

Fatemeh A. Talebi [a], Arash Rabbani [b], Mozhdeh Mehrabi [a], Andrew Stockdale [a], David Harbottle [a], Mehrdad Pasha [a,c], Ali Hassanpour [a,*]

[a] School of Chemical and Process Engineering, University of Leeds, LS2 9JT, United Kingdom
[b] School of Computer Science, University of Leeds, LS2 9JT, United Kingdom
[c] Janssen Pharmaceuticals NV, Turnhoutseweg 30, Beerse 2340, Belgium

## HIGHLIGHTS

- The drop test method is used to measure the adhesion of powders.
- A window of operation for the adhesion measurement using the drop test method is defined.
- Automated image analysis for the detection of the critical particle diameter has been utilised.

## GRAPHICAL ABSTRACT

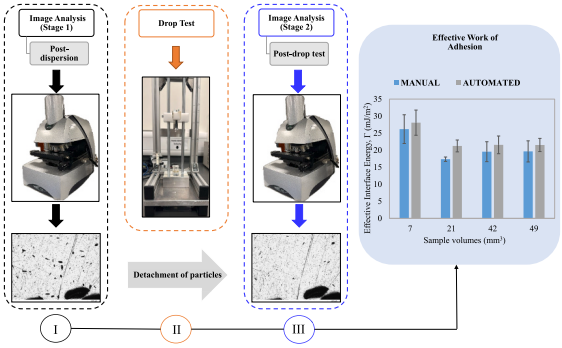


## ARTICLE INFO

*Keywords:*
Particle adhesion
Effective work of adhesion
Critical diameter
Drop test method
Artificial intelligence

## ABSTRACT

Powder adhesion often presents challenges within the pharmaceutical industry as it significantly affects powder flowability and understanding its relationship with powder flow, especially through modelling, presents a major advancement. Traditional approaches such as atomic force microscopy (AFM) and centrifuge method were previously utilised to measure the adhesive force of particles, however, these methods are both time and cost intensive necessitating the need for a more practical solution. This work endeavoured to investigate and develop a window of operation for measuring the effective work of adhesion of both regular and irregularly shaped powders using the drop test method, previously developed at the University of Leeds. For optimisation and accuracy in obtaining the critical diameter of adhesion, the drop test rig was further developed so as to ensure reliable and repeatable measurements of the impact velocity and contact time, which previously posed major challenges. The effective work of adhesion of ibuprofen powders across different sample volumes was measured, to establish a minimum number of analysed particles for ensuring the accuracy of the measured critical diameter. A minimum of 640 ibuprofen particles was required resulting into an effective work of adhesion of 19.6 ± 2.9 $mJ/m^2$. Moreover, the approach was tested on spherical particles, where effective work of adhesion of spherical aluminium-alloy powders (7.7 ± 1.8 $mJ/m^2$) was assessed. Furthermore, artificial intelligence is incorporated in

* Corresponding author.
*E-mail address:* a.hassanpour@leeds.ac.uk (A. Hassanpour).

https://doi.org/10.1016/j.powtec.2024.120605
Received 21 October 2024; Received in revised form 20 December 2024; Accepted 31 December 2024
Available online 3 January 2025

parallel to effectively determine the critical diameter and compare it to the manually calculated values allowing for an efficient image analysis.

## 1. Introduction

Powders often exhibit very complex and unpredictable bulk-scale behaviour resulting into challenges associated with particulate processes in the pharmaceutical industry. Powder flowability is a crucial factor for the success of several pharmaceutical processes such as mixing/blending, capsule filling and coating [1–3]. It is commonly known in literature that poor flow behaviour of powders often results into variable tablet or capsule weights, unacceptable content uniformity and ultimately posing an obstacle in manufacturing [1–4]. Specifically, active pharmaceutical ingredients (API) such as ibuprofen (IBU) powders are known to be problematic due to their high surface adhesion, irregular morphology and their high demands for solubility, which requires very fine sizes thus increasing their propensity to agglomerate [5–7]. High surface adhesion and irregularly fined shaped particles are often associated with poor flow which consequently limits the continuous production processes by inhibiting smooth powder handling and processing [8].

An in-depth understanding of a powder's adhesion properties is expedient to predict powder flow, which is of great importance within pharmaceutical applications so as to ensure products meet the desired specification [9,10]. Understanding the correlation between adhesion and powder flow is a major step forward and can be established using modelling, particularly through Discrete Element Method simulation (DEM) [11]. DEM requires a range of input parameters such as particle adhesion, where is usually inserted as single values based on the applied contact model such as the Johnson-Kendall-Roberts (JKR)-based contact theory [12,13]. While majority of researchers use the "calibration method" [14] there are limited work that have indeed implemented measured properties, such as adhesion [11]. Furthermore, challenges such as sticking, which is associated with adhesion problems during tablet manufacturing, often presents itself towards the end of the development process [15,16]. This calls for the need to be able to numerically predict if a new formulation may exhibit adhesion problems earlier in the research and development stage [15]. The lack of computational models to predict powder flow in regards to particle adhesion poses a great challenge within the process development stages [17]. By effectively measuring the particle adhesion, the powder flow can be predicted by utilising DEM, which can optimise and enhance pharmaceutical powder processing.

Particle adhesion as an inherent powder property is defined as the attraction between two solid entities as a result of forces acting over a distance [18]. A range of interactions such as mechanical interlocking, van der Waals and electrostatic forces further addresses particle-particle and particle-surface adhesion. The particle-surface adhesion as a result of these interactions generates variable flow, which is undesirable in the pharmaceutical industry as it impacts dose uniformity and the quality of the end product.

Adhesive force measurements can be categorised on the premise of their particle-detachment action. The first category accounts for methods that consist of the detachment of a large quantity of particles, where the detachment force "acts simultaneously on all the adherent particles present on the surface" [19]. These methods include the centrifugal, vibrational, and impact techniques, while the second category consists of methods that only measure the detaching force acting on a single particle and not propagated to adherent particles such as the atomic force microscopy (AFM) [20–23]. Additionally, Zhang et al. [24] first introduced a novel micromanipulation technique for measuring the mechanical strength of single cells, which was further developed to directly measure the adhesive strength of biofilms through a T-shaped probe [25]. It is important to note that the results obtained from these techniques varies due to the individual mechanisms involved such as differences in powder deposition, surface contact measurements and strain rate [26]. Atomic force microscopy (AFM) that is widely used to measure the adhesive force of particles, utilises a colloidal probe measurement, where a single particle is attached to the end of a microcantilever, limiting the number of particles analysed. Due to the single point measurement on a surface, AFM does not take into account the effective particle-particle-wall contact area nor does it provide an average property of particles. The centrifuge method faces limitations as well, since the resulting adhesion force distributions are influenced not only by the adhesion mechanism and contact geometry but also by the particle size distribution, which must be kept as narrow as possible to minimise this effect [27,28]. Additionally, the centrifuge method is associated with inflexibility for the operator due to the immobile and heavy nature of the equipment [29]. Moreover, the aforementioned techniques are not only costly but also time-consuming, necessitating the development of more efficient solutions.

The impact techniques such as the studies conducted by Ermis et al. [29], Zafar et al. [30], Deng et al. [28] and Pedrolli et al. [31] have provided solutions to tackle the challenges associated with the traditional techniques such as eliminating single particle analysis that is both time and cost efficient. Ermis et al. [29] developed a novel "impact adhesion tester" to measure particle adhesion strength of food particles on food surfaces. They compared their finding with the centrifuge method and concluded that the adhesion forces calculated from both techniques were very close in magnitude and in agreement with each other [29]. Zafar et al. [30] developed the "drop test" technique to measure the interfacial particle adhesion based on the Johson, Kendall and Roberts (JKR) model of adhesion [12] and Newton's second law of motion. They conducted an experimental study by adhering particles on to an aluminium substrate and subjecting them to a tensile force by dropping them at a set height onto a stopper ring. The detachment force of each particle was calculated using the mass particle, impact velocity and the contact time during detachment. From the balance of the detachment and adhesive force for a critical diameter size, above which particles detach from the substrate and below which powders adhere onto the surface, the interfacial specific energy was calculated. The material they utilised in their experiments were salinized glass beads, starch, Avicel and α-lactose monohydrate. However, their drop test primarily focused on spherical particles, with limited methodology for irregular particles, which presents significant challenges in measuring particle adhesion. Furthermore, one of the limitations of the set-up was the measurement of contact time during detachment which was central for the calculation of adhesion force. Deng et al. [28] conducted a study of particle adhesion for cohesive powders using the novel "mechanical surface energy tester" and Bond number on tablet substrate powders such as paracetamol, ibuprofen, lactose and calcium carbonate. They calculated the adhesion force based on an assumption that this force is equivalent in magnitude, but opposite in direction to the deceleration force at detachment. Similar to the drop test the particles are adhered on a substrate, which is halted against a stopper, where the detached particles are collected and measured for total mass [28]. The study concluded that particle adhesion for cohesive powders can be analysed in terms of particle size, with the Bond number used to represent powder cohesiveness. Additionally, they noted that particle-surface adhesion is influenced more by the particle properties, or "particle deposition status," rather than by the material's surface [28]. Although an accelerometer was used to obtain a wide range of acceleration values and compare them with the total mass of detached particles, relying solely on the total mass of detached particles may not accurately indicate the critical diameter of a material. Moreover, Pedrolli et al. [31] presented a

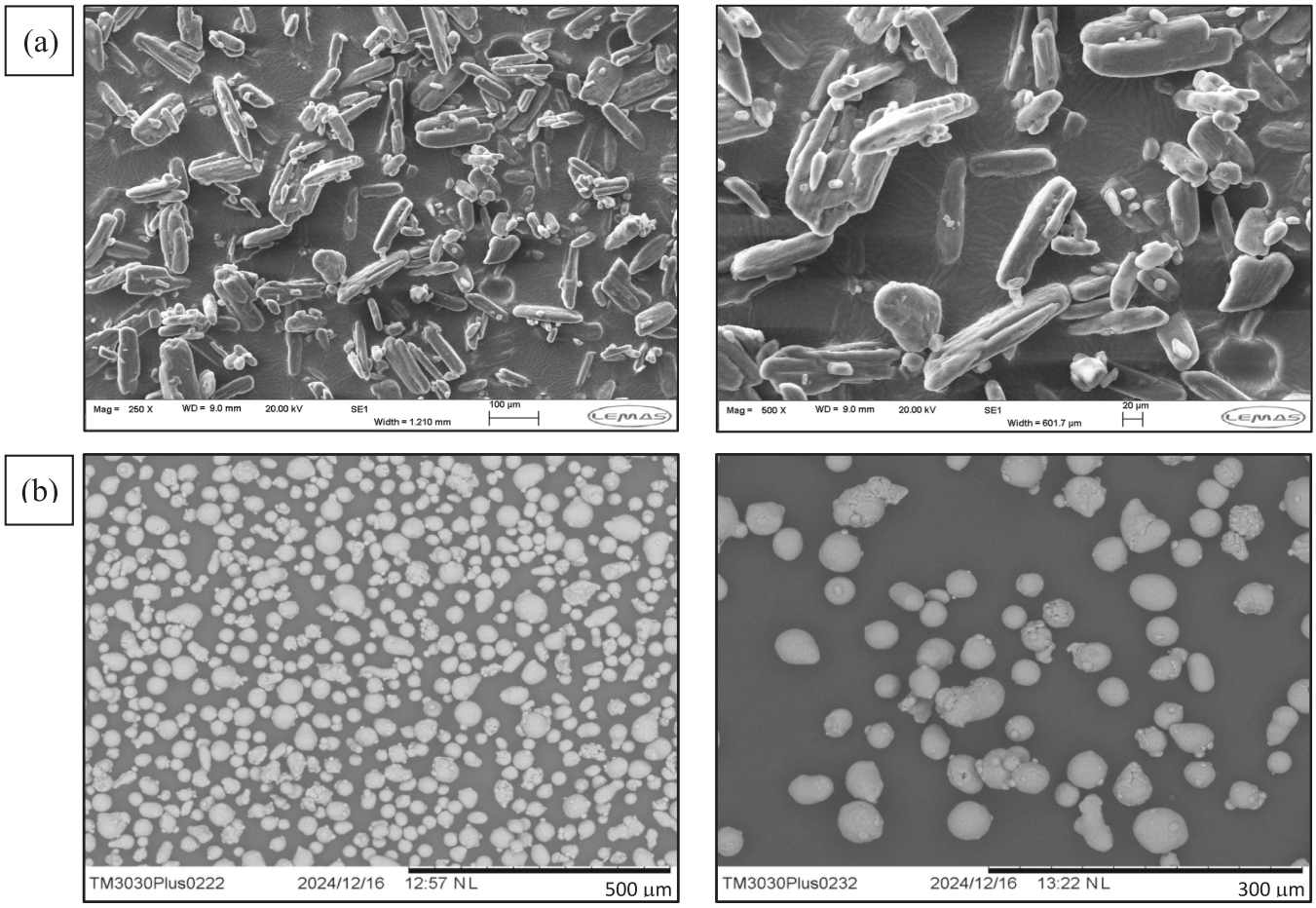


**Fig. 1.** Scanning electron microscope (SEM) images of (a) ibuprofen and (b) aluminium-alloy powders.

novel interpretation of the JKR model allowing for the development of a test procedure by using a novel "kinetic adhesion test" using stainless steel, borosilicate glass and UPVC film. The "kinetic adhesion test" was developed to determine particle surface energy in a streamlined procedure at a time and cost-effective manner [32]. Their work was also based on the balance between the kinetic and adhesive energy for the determination of the mesoscale adhesive energy, which was experimentally verified through the measurements of the contact radius [31]. Their method aimed at DEM simulations which enabled modelling the behaviour of cohesive powders through the adhesive energy value using the JKR contact model. By utilising the"kinetic adhesion test", the values for the adhesive energy were calculated promptly and with ease to be used in simulations where the microscopic interactions are not modelled [31]. The kinetic adhesion test was based on a magnetic release mechanism of the sample carrier, which could be subject to wobbling during impact due to the air drag.

The aim of this work is to measure the effective work of adhesion of irregularly shaped ibuprofen powders and spherical aluminium-alloy powders by employing the drop test technique, which was first introduced by Zafar et al. [30]. In this paper, we aim at developing a more systematic methodology for the particle adhesion force measurement using the drop test technique. To optimise and accurately calculate the critical diameter, the in-house drop test has been further developed to minimise errors associated with impact velocity and contact time during detachment, which were previously measured using a high-speed camera. In addition, our work endeavours to provide a systematic methodology for calculating the effective work of adhesion for both spherical and irregularly shaped particles. According to the best of our knowledge, adhesion measurement of irregularly shaped particles have not been extensively investigated in literature, especially in regards to a systematic methodology. Furthermore, establishing a minimum volume of sample (associated with the analysed particle number) is imperative, as falling below this threshold significantly compromises the accuracy of the measured critical diameter. Moreover, artificial intelligence is incorporated in parallel to effectively determine the critical diameter and compare it to the manually calculated values allowing for an efficient image analysis.

## 2. Methodology and experimental procedure

### 2.1. Materials

Ibuprofen, an active pharmaceutical ingredient, is used as the model material in this study. The ibuprofen powders crystallised in hexane and supplied by BASF was dispersed on a polished aluminium substrate with a diameter of 15 mm. Fig. 1 below demonstrates the scanning electron microscope (SEM) images of the ibuprofen particles characterised by needle shaped morphologies and agglomerates due to the presence of strong inter-particle forces. Additionally, aluminium-alloy powders characterised by a $D_{50}$ of 45 µm was used as a secondary material to investigate and test the application of the method on spherical particles. Fig. 1(b) displays the scanning electron microscope (SEM) images of aluminium-alloy particles that exhibited regular, spherical morphologies.

Morphologi G3® is an advanced particle size and shape characterisation tool or in other words, an automated optical microscope with a software package that enables the measurement of particle size and shape based on two dimensional image capture [33]. Based on the

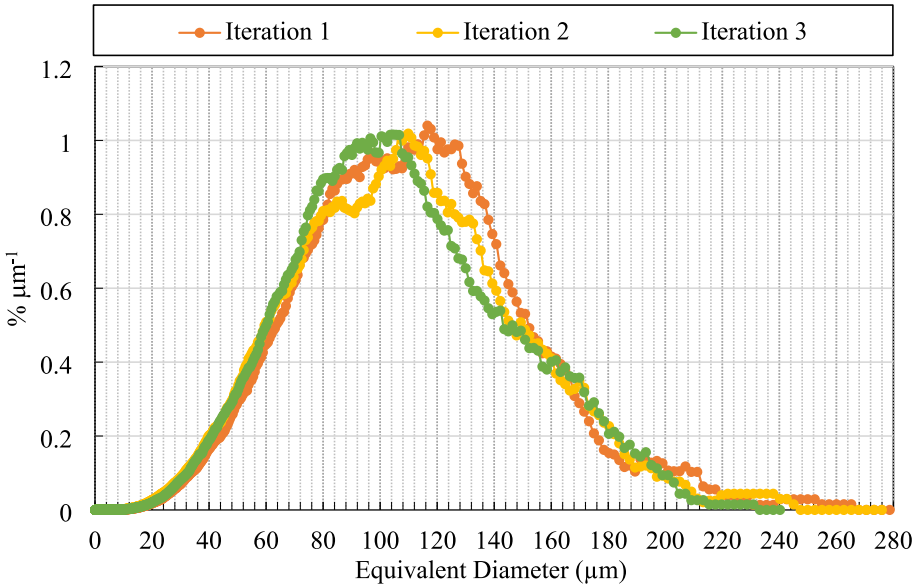


**Fig. 2.** Volume based particle size distribution of the ibuprofen powders.

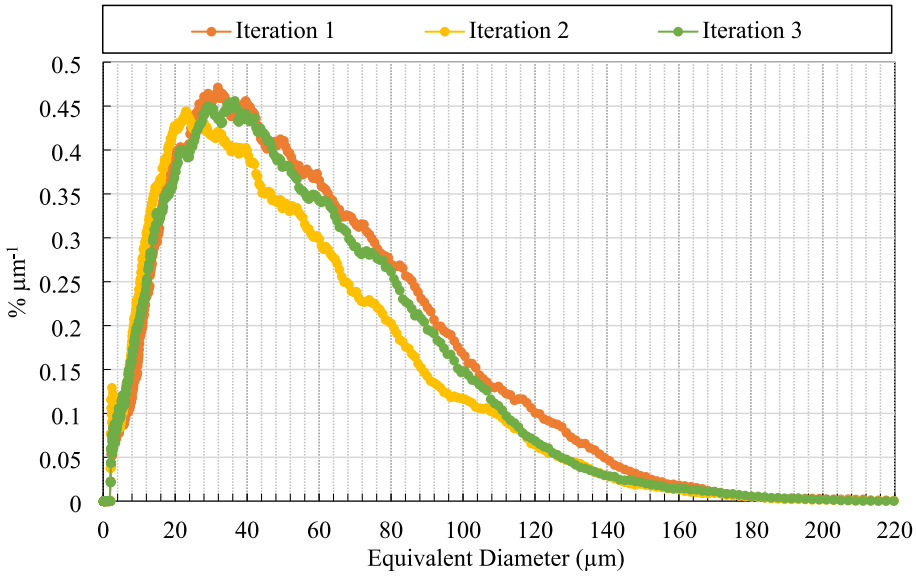


**Fig. 3.** Number based particle size distribution of the ibuprofen powders.

simple principle of an optical microscope, a transmitted or reflected light is used to generate an image, where the objective lens collects the lights passing through the particle, generating a magnified image. Additionally, characterising a three dimensional (3D) particle often poses major bottlenecks, hence for practicality and consistency, it is convenient to describe particle size as a single number such as the Circle Equivalent (CE) diameter [33]. The image analysis involves the two dimensional (2D) image capture of a 3D particle. The Morphologi G3® evaluates the Circle Equivalent (CE) diameter of a circle with the same projected area as the 2D image of the particle. Fig. 2 and Fig. 3 below demonstrates the volume and number based particle size distribution of the ibuprofen powders by utilising the Morphologi G3®, respectively. This illustrates that the sample consists of a wide particle size distribution. The reason for the particle size distribution not exhibiting a smooth trend across the three iterations may be due to the wide range of particle sizes present, especially in samples consisting of very fine particles or agglomerates [34]. Furthermore, the number of particles present for each test may also cause variations in the smoothness of the graphs due

**Table 1**
Volume based particle size distribution of ibuprofen powders.

| | D[v, 0.1] (µm) | D[v, 0.5] (µm) | D[v, 0.9] (µm) |
|---|---|---|---|
| Iteration 1 | 50 | 95 | 147 |
| Iteration 2 | 46 | 91 | 146 |
| Iteration 3 | 47 | 90 | 146 |

**Table 2**
Number based particle size distribution of ibuprofen powders.

| | D[n, 0.1] (µm) | D[n, 0.5] (µm) | D[n, 0.9] (µm) |
|---|---|---|---|
| Iteration 1 | 7 | 29 | 77 |
| Iteration 2 | 6 | 23 | 67 |
| Iteration 3 | 6 | 27 | 73 |

**Table 3**
Shape factors ibuprofen powders.

| | Iteration 1 | | | Iteration 2 | | | Iteration 3 | | |
|---|---|---|---|---|---|---|---|---|---|
| | D[n, 0.1] | D[n, 0.5] | D[n, 0.9] | D[n, 0.1] | D[n, 0.5] | D[n, 0.9] | D[n, 0.1] | D[n, 0.5] | D[n, 0.9] |
| Circularity | 0.42 | 0.72 | 0.91 | 0.47 | 0.76 | 0.93 | 0.44 | 0.74 | 0.92 |
| Aspect Ratio | 0.31 | 0.52 | 0.79 | 0.32 | 0.54 | 0.8 | 0.32 | 0.53 | 0.8 |
| Elongation | 0.2 | 0.48 | 0.69 | 0.2 | 0.46 | 0.68 | 0.2 | 0.46 | 0.68 |
| Convexity | 0.9 | 0.99 | 1 | 0.92 | 0.99 | 1 | 0.9 | 0.99 | 1 |

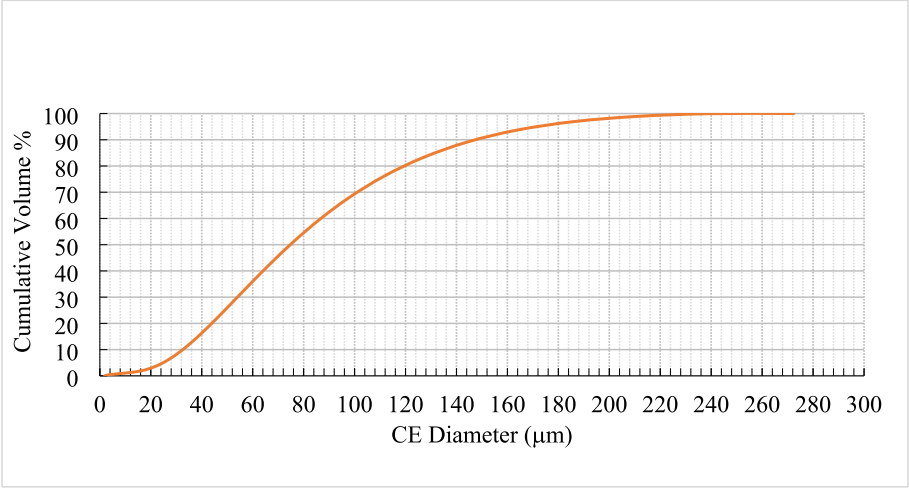


**Fig. 4.** Cumulative volume based particle size distribution of the ibuprofen powders using laser diffraction.

**Table 4**
Volume based particle size distribution of ibuprofen powders using laser diffraction.

| | D[v, 0.1] (μm) | D[v, 0.5] (μm) | D[v, 0.9] (μm) |
|---|---|---|---|
| Iteration 1 | 38 | 86 | 170 |
| Iteration 2 | 38 | 87 | 174 |
| Iteration 3 | 38 | 86 | 169 |

to sample-to-sample variations. Table 1 and Table 2 provides further information of the volume based and number based particle size distribution of the ibuprofen powders over three iterations. It can be deduced that the information of the particle size distribution obtained by the Morphologi G3®, correlates well with the particle sizes portrayed on the SEM images in Fig. 1(a). Table 3 summarises the shape factors such as circularity, aspect ratio, elongation, and convexity obtained for the ibuprofen powders using the Morphologi G3®. Convexity is a measure of a particle's surface roughness and values that approach 1 suggests that particles exhibit a "spiky" or rougher surface [33], which is evident in Fig. 1(a). Elongation values closer to 1 suggests that particles are elongated resembling a rod which is also depicted in Fig. 1(a). Aspect ratio and circularity values approaching 1 indicates that particles are closer to the shape of a sphere, however, it also indicates symmetrical particles. It is imperative to note that a single shape factor is insufficient to fully characterise a single particle, hence an understanding of the combination of these shape factors is essential to accurately describe and characterise the particles.

Additionally, Mastersizer 3000 ®, which is a laser diffraction particle size analyser was utilised to measure the particle size distribution of the ibuprofen. The wet method was utilised where the sample was prepared by mixing 2.5 g of ibuprofen powder in 50 mL of Milli-Q water. This was left on the stirrer for 10 min to ensure adequate mixing. A pipette was then utilised to pour the sample in the instrument until reaching a sufficient obscuration level. Fig. 4 provides the cumulative volume based particle size distribution and Table 4 summarises the particle size distribution obtained from the Mastersizer 3000 ®. The particle size distribution obtained from the Morphologi G3® and Mastersizer 3000 ® are correlated and have an acceptable variation, which is a result of the differences in the techniques utilised by the two instruments.

Furthermore, the surface topography of the aluminium substrate was examined using a Bruker-NPFlex Surface 3D Optical Profilometer. Fig. 5 (a) illustrates the surface of the substrate before applying the Gaussian Regression filter, while Fig. 5(b) depicts the surface measurements after applying the Gaussian Regression filter which result into the following roughness parameters: peak ($S_P$), valley ($S_v$) and mean ($S_a$) values of 2.2 μm, -3.5 μm and 0.03 μm, respectively. Fig. 5(c) portrays the 3D view of the substrate where the scratches are evident, which is due to the limitations posed by the available polishing instrument. It is important to note that, although the roughness values are significantly smaller than the particle sizes, they can influence the particle-substrate contact area and consequently the adhesive properties.

### 2.2. Development of the drop test rig

The drop test measures the effective work of adhesion, $\Gamma$, of particles by subjecting them to a dynamic tensile force. The effective work of adhesion, $\Gamma$, is then calculated by balancing the detachment force (as described by Newton's second law of motion) and the adhesive force (as per the JKR model of adhesion) for a critical particle size of a given sample [30]. Theoretically, particles smaller than a critical size will remain attached, while those larger will detach from the surface of the substrate to which they adhered on. The "critical diameter" is the diameter of an imaginary particle that has an adhesion force equal to its detachment force and is assumed to lie in the range of the particles still adhered on the substrate after the drop test and the detached particles.

The original drop test set-up, developed by Zafar et al. [30] was further upgraded for the following purposes:

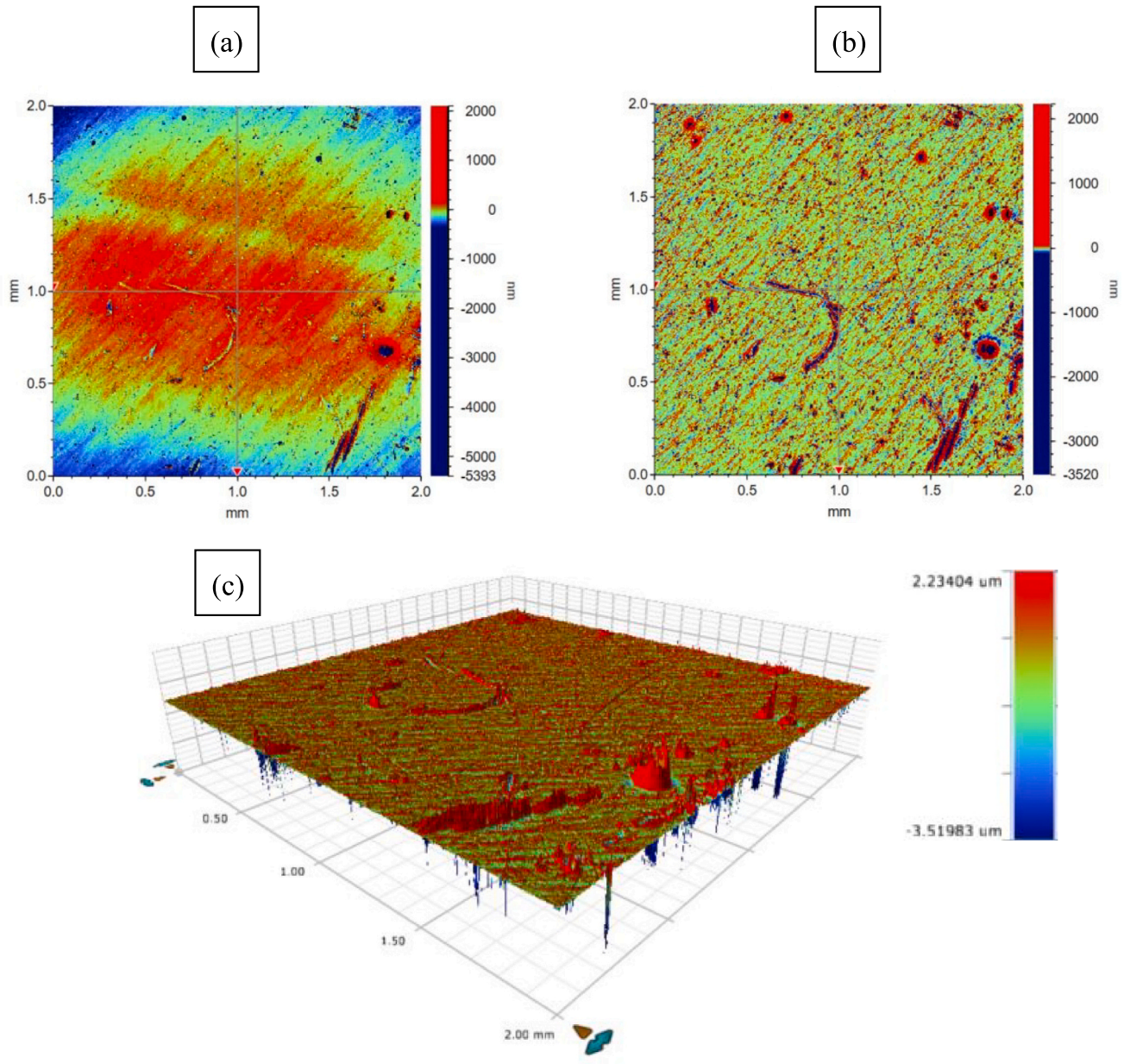


**Fig. 5.** Surface topography measurements of the substrate using the NPFlex Surface 3D optical Profilometer, where (a) and (b) is the substrate before and after applying the Gaussian Regression filter, respectively. Fig. 5(c) is the 3D profile of the substrate.

1- The initial design was prone to the wobbling effect where the substrate was manually dropped. To mitigate this effect, parallel bearing bars was utilised to allow the dropping platform travel down without any significant friction or vibration. The substrate was fitted on the dropping platform using a butterfly screw and released through the release mechanism in Fig. 6(b), ensuring that the dropping platform carrying the substrate is dropped at a precise and consistent manner, allowing it to land directly on top of the stopper stage without any tilt or misalignment. This ensures even tensile force distribution across the particles. A video of how the dropping platform travels down and impacts the stopper stage can be found in Appendix D.
2- A high-speed camera was previously used to calculate the contact time during detachment, which was not only time consuming as it required a separate set-up but also resulted into inaccuracies due to the limitations of the camera's operating window. To eliminate these challenges, a piezoelectric ring was positioned on top of the stopper stage and held in place with a holder as depicted in Fig. 6(d) so as to measure the contact time upon impact at a reliable and repeatable manner.
3- The impact velocity was also measured using the high-speed camera in the previous design, resulting into inaccuracies associated with its set-up and analysis. To ensure repeatable and reliable results, photomicrosensors were implemented to measure the impact velocity in a controlled and automated manner. Fig. 6(a) depicts the position of the photomicrosensors.

Fig. 6 illustrates the schematics of the upgraded in-house drop test rig.

### 2.3. Set-up and methodology of the drop test

Establishing a standard operating procedure for measuring the effective work of adhesion using the drop test is imperative for the accuracy, reliability and the statistical robustness of the results. The major challenge is associated with the quantity of APIs available, restricting

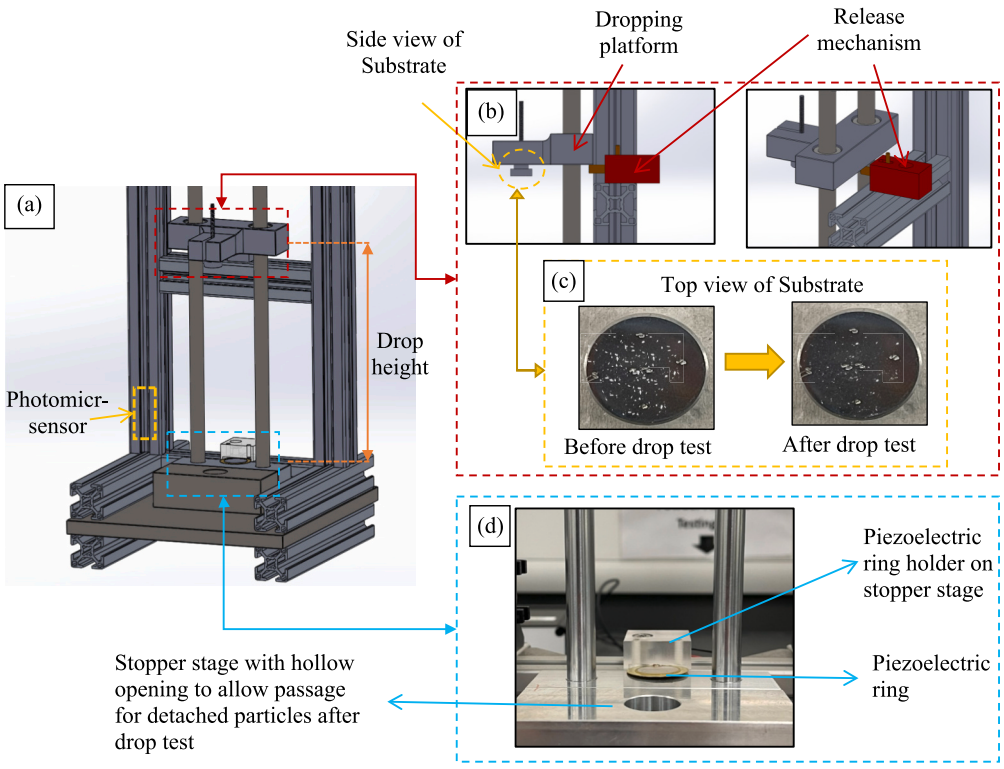


**Fig. 6.** (a) Schematic drawing of the overall drop test rig with position of the photomicrosensors, (b) the release mechanism to disengage the dropping platform carrying the substrate, (c) the top view of the substrate depicting the particles dispersed on the surface before the drop test and the remaining particles that remained attached after the drop and (d) the stopper stage consisting of two blocks where the one in front consists of a hollow opening to allow passage for the detached particles after the drop, while the block behind provides a surface to position the piezoelectric ring held by a holder.

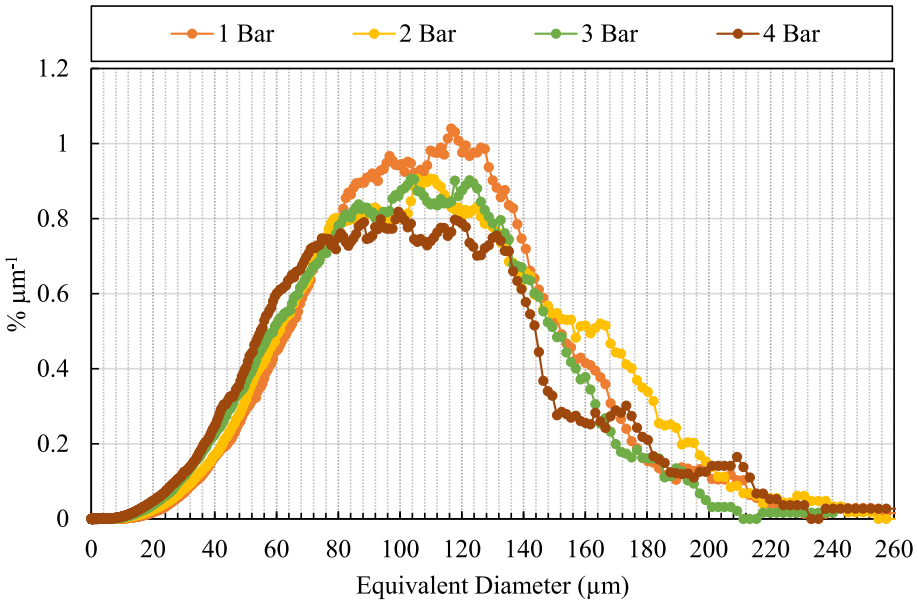


**Fig. 7.** Volume based particle size distribution of the ibuprofen powders at different dispersion pressure.

the use of traditional characterisation techniques, which require a larger amount of sample. However, despite the limited availability of samples, it is essential to establish a threshold below which the accuracy of results is significantly compromised. This underscores the need to develop a standardised operating procedure which is dependent on the particle size distribution of a sample. The experimental work involved using the drop test rig to measure the effective work of adhesion of the ibuprofen powders across four different sample volumes: 7 $mm^3$, 21 $mm^3$, 42 $mm^3$, and 49 $mm^3$ based on the available Morphologi G3® spatulas with set volumes. The samples were dispersed onto an aluminium substrate at a dispersion pressure of 1 bar using the Morphologi G3®. 1 bar was used as it ensured that there was no particle breakage. Fig. 7 and Fig. 8 illustrates the volume based and number based distribution of the sample dispersed at four different pressures. It is evident that as the pressure increases, the number of finer particles increases suggesting that the increase in pressure breaks the particles between approximately 80 µm

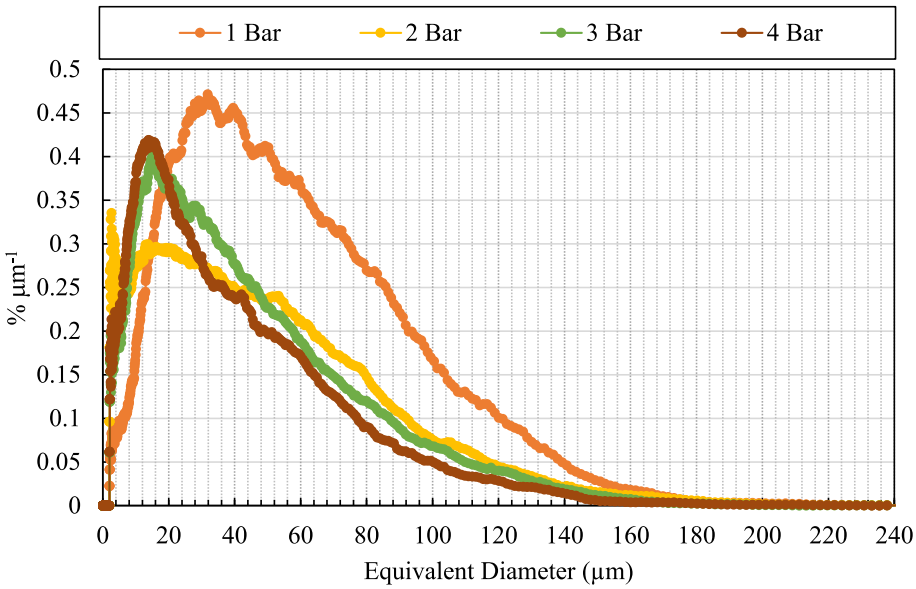


**Fig. 8.** Number based particle size distribution of the ibuprofen powders at different dispersion pressures.

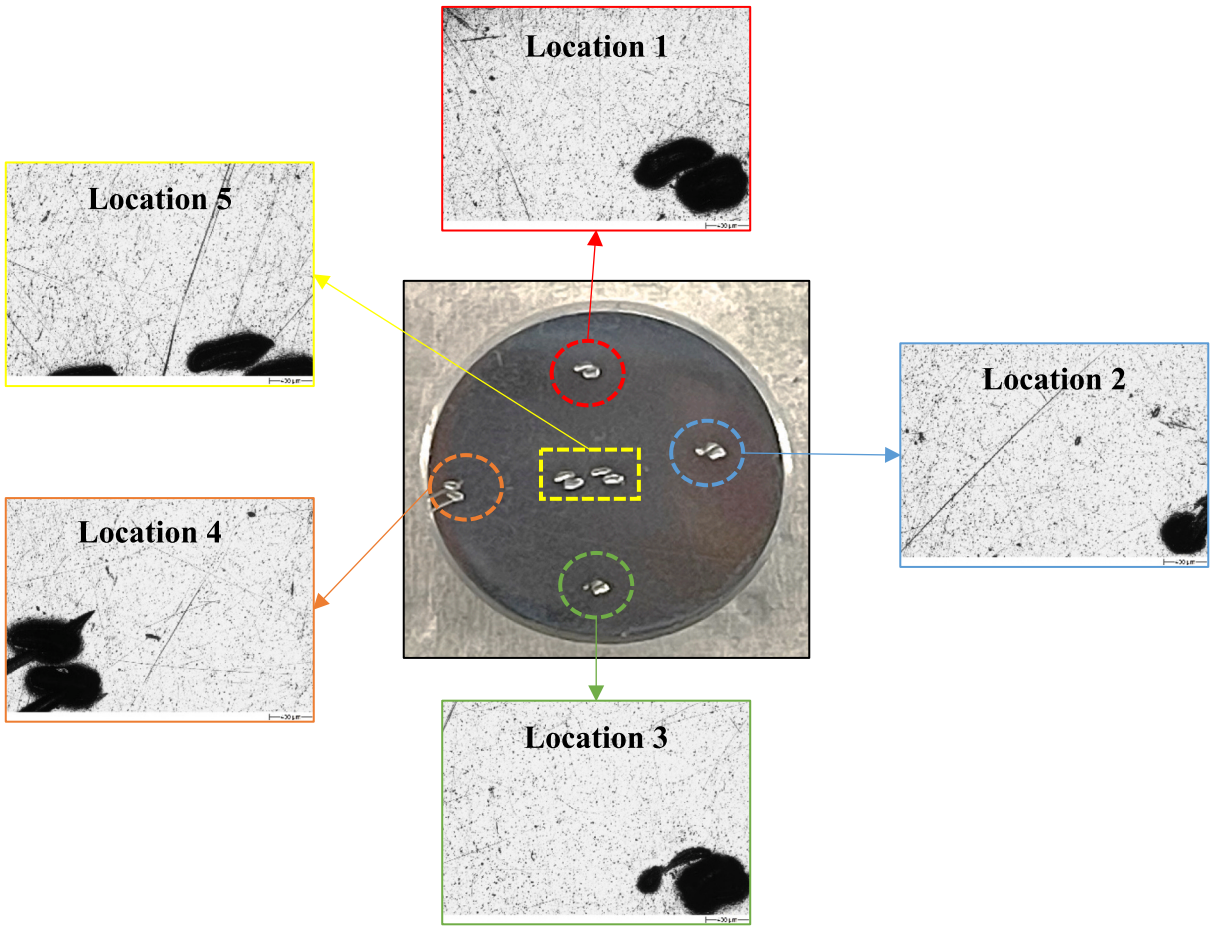


**Fig. 9.** Substrate made of polished aluminium stub divided into five areas namely; location 1, 2, 3, 4 and 5 for image analysis. Note: the large black marks on the images are the reference points.

to 140 µm. Additionally, it is evident in Fig. 7 that the fraction of particles above 145 µm at 2 bar is more than at 1 bar, which may be a result of several factors such as batch to batch variation of the powder sample deposited and effects of particle orientation, which impacts particle size measurements due to the variations in the projected area. Furthermore, particle interlocking as a result of irregular particle morphologies may result into clusters and agglomerates at 2 bar. It is evident from Fig. 8 that for particles below 6 µm, there is an increase in the finer particles at

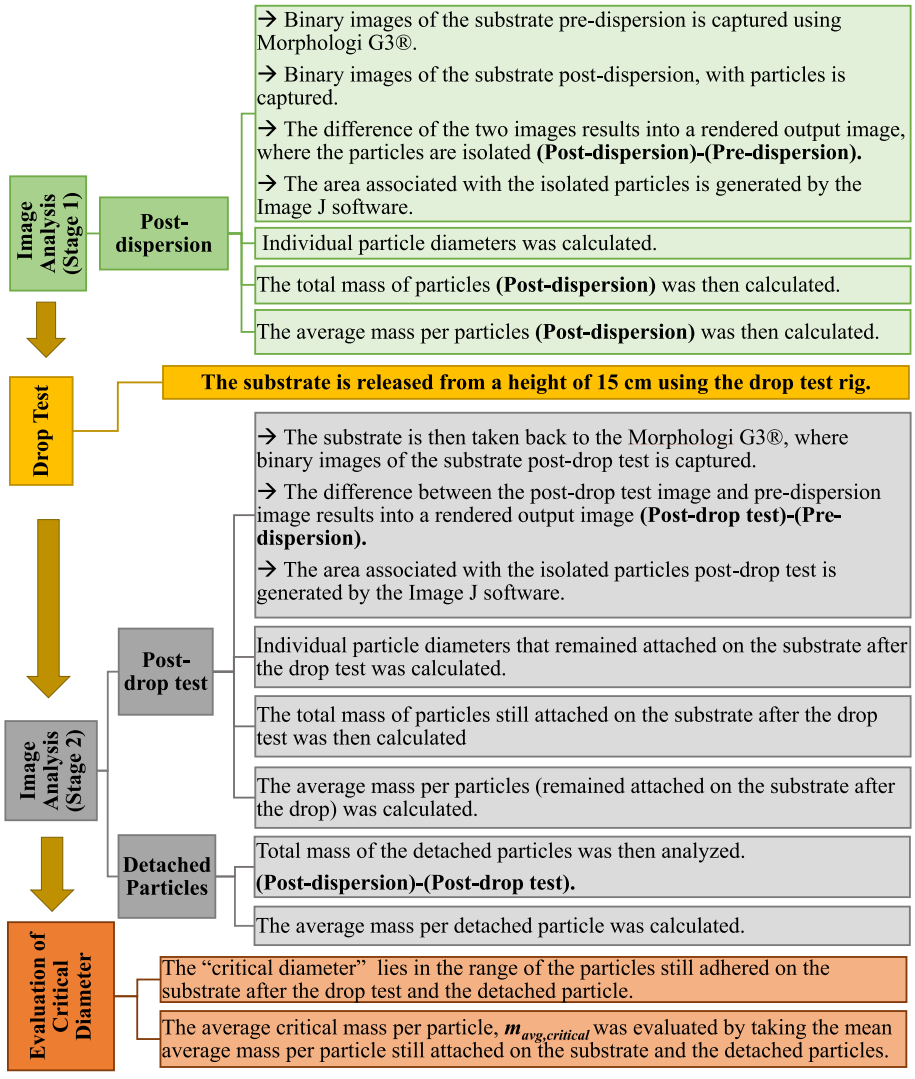


**Fig. 10.** Simplified flow chart for manually isolating the critical diameter.

2 bar. It is important to note that this peak is only detected on the number based distribution and is negligible on the volume based distribution. Generally, higher pressure bars are not advised as they change the inherent particle size and morphological characteristics, hence why the choice of 1 bar was utilised in this study.

The temperature and humidity were at ambient lab conditions, which ranged from 21.1 °C to 24.6 °C and 43 % to 61 %, respectively.

This section provides a step-by-step explanation of the experimental procedure:

1. A substrate with a detachable screw should be utilised as a surface for powder adhesion. In this work a polished aluminium SEM stub was used as the substrate. It was divided into five areas, labelled as locations 1, 2, 3, 4, and 5 as illustrated in Fig. 9 below, providing reference points for ease of analysis and identifying particle orientation.

   It is important to note that the colour variations observed in the overall aluminium substrate and its five areas are due to the binarized images captured by the Morphologi G3®.
2. The substrate was then placed under the microscope of the Morphologi G3®, where images of each location were captured before dispersion. This was done so instead of scanning the entire area of the substrate which leads to inaccuracies in particle detection as the edges of the particles can be distorted due to the pixelated nature of the scan area generated as a direct output from the Morphologi G3® software. By dividing the substrate into five areas, a representative and accurate particle detection through image analysis can be undertaken where the exact orientation and nature of particles can be detected. A scale of 1 pixels/μm was implemented for all the images.
3. All the images captured were of the same focal length and exposure- lighting so as to ensure that the images were identical for analysis.
4. For the experiment, the substrate should always be positioned in the same location on the stage to ensure consistency within the dispersion area. The air dispersion is then set, and particles are dispersed onto the substrate.
5. After dispersion, exact images of each of the five areas with the same magnification were captured. The reference points enabled exact locations and orientation of particles to be detected.
6. The substrate was carefully positioned onto the screw using a pair of tweezers and then transferred to the drop test rig. To prevent contamination and external forces such as drag during transportation, the substrate was placed inside a glass jar cover.
7. The substrate with the dispersed powders was then carefully attached to the dropping platform (Fig. 6(b)). A drop height is then adjusted (Fig. 6(a)) and the dropping platform is released using the release mechanism (Fig. 6(b)). It should be noted the

drop height should be chosen based on the adhesive properties of particles in a way that enough number of particles would remain attached to the substrate after the test for the analysis. For the samples in this work, we shall stick to a 15 cm and 10 cm drop height for the ibuprofen and aluminium-alloy powders, respectively. Upon impact of dropping platform with the stopper stage at the bottom of the rig (Fig. 6(d)), the particles on the surface of the substrate experience tensile stresses, resulting particles larger than a critical diameter to detach (Fig. 6(c)).

8. The impact velocity was measured using photomicrosensors, which were positioned at an exact gap of 2.00 cm (Fig. 6(a)). Upon release and the initiation of the drop, the two sensors were able to detect the movement of the dropping platform. The photomicrosensors which were attached to a PicoScope® 2000 Series Oscilloscope generated an output in the form of a graph of voltage against time. This will be further explained in section 2.6, step 1.
9. In parallel, upon impact of the dropping platform onto the piezoelectric ring, the contact time was measured. The piezoelectric ring was also attached to another PicoScope® 2000 Series Oscilloscope where the output was generated simultaneously. This will be further clarified in section 2.6, step 2.
10. The substrate was then carefully removed and positioned back under the Morphologi G3®, where images of the post drop test for each of the locations were captured.
11. Three iterations for each sample volume was undertaken. The Morphologi G3® and the drop test rig were thoroughly cleaned to avoid cross contamination. The electrostatic charging on the surfaces of the equipment and substrate was mitigated by wiping them with anti-static spray.

### 2.4. Image analysis- manual isolation of the critical diameter

The accurate calculation of the critical diameter on the substrate is imperative in this work. The binary images of the substrate before and after the drop test (Fig. S. 1(b) and (c), respectively in the Supplementary Data S1: Appendix A) obtained from Morphologi G3® were used to obtain the moment based critical particle size with the aid of the open-source software, Fiji [35]. Images from each of the five locations (Fig. 9) are analysed individually and then combined to identify the population and distribution of the ibuprofen and aluminium-alloy particles on the substrate, post-dispersion and post-drop test (See Fig. S. 2(a-d), in the Supplementary Data, S1: Appendix A). The area of the particles generated were then converted to individual particle diameters ($d$, μm), which were then used to calculate the total mass (m) of particles. It should be noted that in this study the mass of particles on the substrate are under 1 μg, hence it was not feasible to conduct an accurate gravimetric measurement. The Rice Rule [36] (Supplementary Data, S1: Appendix A, Eq. S. 2) was utilised for calculating the bin size and the number of bins required for a given number of observations, which is required for calculating the total mass (m) of particles in each bin size (Supplementary Data, S1:Appendix A, Eq. S. 3). The average mass of particles, post-dispersion and post-drop tests was then calculated. Herein, the mean of the average mass per particle still adhered post-drop test and the average mass per detached particle are calculated to evaluate the average critical mass per particle, $m_{avg,critical}$, i.e. the mass of particle with "critical diameter" (Supplementary Data, S1:Appendix A, Eq. S. 5). The detailed methodology on how the critical diameter is manually isolated can be found in the Supplementary Data, S1: Appendix A.

Fig. 10 below demonstrates a simplified flow chart, which summarises the steps taken to calculate the critical diameter. The entire process is divided into four phases, namely; post-dispersion image analysis (stage 1), drop test, post-drop image analysis (stage 2) and the evaluation of the critical diameter. Post-dispersion image analysis (stage 1) involves the necessary steps undertaken for isolating the particles initially dispersed on the substrate. The drop test is then undertaken which then leads to the third phase; post-drop image analysis (stage 2) where the particles that remain attached on the substrate after impact are isolated. It should be reiterated that the criterion for calculating the critical diameter is based on the assumption that this value falls within

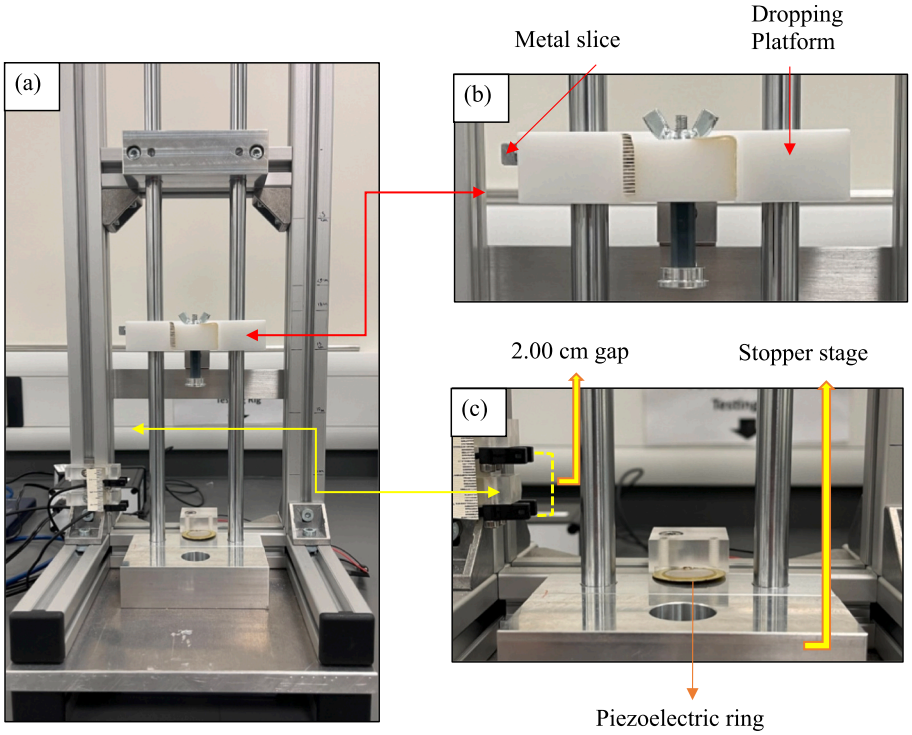


**Fig. 11.** (a) Overview of the drop test rig, (b) dropping platform carrying the substrate with metal slice attached, and (c) positioning of the piezoelectric ring and photomicrosensors at a gap of 2.00 cm.

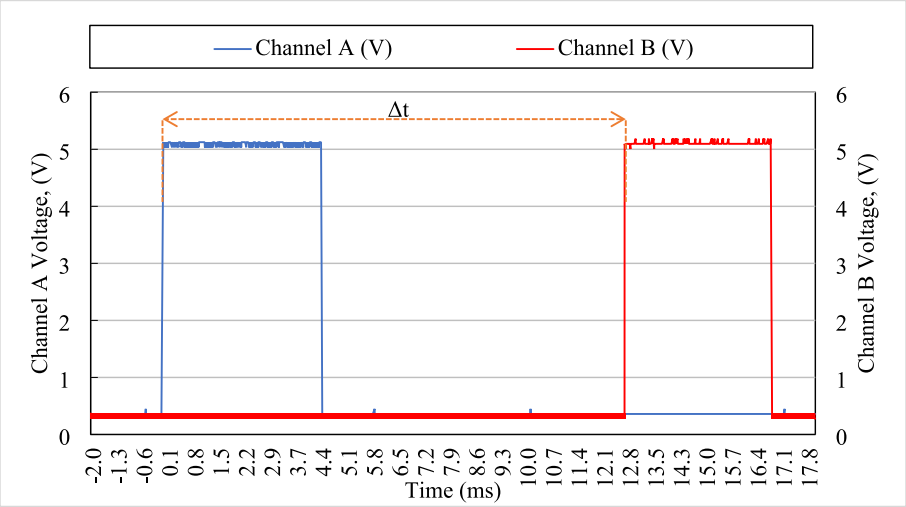


**Fig. 12.** PicoScope® 2000 Series Oscilloscope generating output for the time taken by the dropping platform to travel between the photomicrosensors.

the range of particles that remain adhered to the substrate after the drop test and those that detach. Having an understanding of the critical diameter, will allow an indication of the adhesive properties of a sample in regards to particle-surface interactions.

### 2.5. Automated measurement of the critical diameter

An automated image analysis algorithm was developed as an alternative approach to determine the critical diameter of particles for adhesion calculation. The algorithm comprises three sequential stages: image registration (Supplementary Data, S2: Appendix B, Section S2.2,), particle segmentation (Supplementary Data, S2: Appendix B, Section S2.4), and statistical analysis (Supplementary Data, S2: Appendix B, Section S2.5). The image registration process utilises an intensity-based automatic registration technique [37,38] to align the post-dispersion and post-drop test images with the pre-dispersion reference image. For particle detection, the algorithm applies intensity-based thresholding of difference images followed by watershed segmentation on the Gaussian-smoothed distance transform to identify individual particles [39–43]. The particle size distributions are then computed using equivalent diameters calculated from the area of each segmented region.

The algorithm employs various optimization techniques including the "One Plus One Evolutionary" optimizer [37] for image registration and morphological operations for noise reduction (Fig. S. 3(a-f) in the Supplementary Data, S2: Appendix B). The process includes automatic filtering of particles smaller than a minimum area threshold to exclude surface artefacts, and detection of agglomerates through adjacency analysis of segmented regions. Statistical analysis of the particle size distributions enables calculation of the critical diameter using the momentum-weighted averaging of the size distributions for remained and dropped particles (Supplementary Data, S2: Appendix B, Section S2.5).

The detailed implementation of the automated measurement methodology, introduction of the machine vision terminology, and justifications of algorithmic design choices are provided in Supplementary Data, S2: Appendix B.

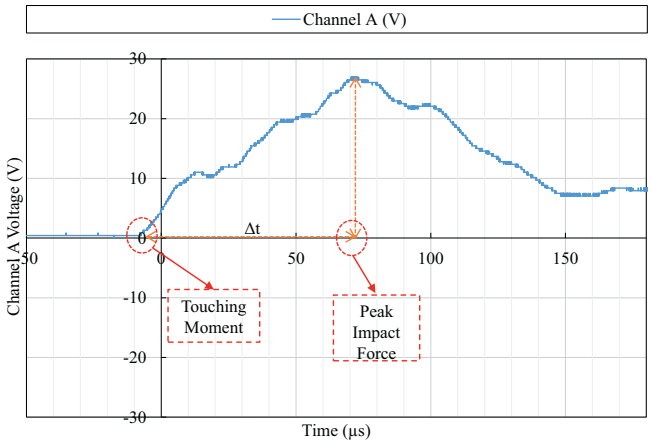


**Fig. 13.** PicoScope® 2000 Series Oscilloscope generating output from the impact of the dropping platform on the piezoelectric ring to calculate the contact time.

### 2.6. Particle adhesion, impact velocity and contact time

This section will further elucidate the methodology employed for calculating the particle adhesion, impact velocity and contact time using the JKR theory as a model of adhesion and Newton's second law of motion for the detachment force [12]. The contact time and impact velocity were calculated using the piezoelectric ring and photomicrosensors that were connected to a PicoScope® 2000 Series Oscilloscope (Supplementary Data, S3: Appendix C) that detected the signals and generated output through the "PicoScope 7 T&M" and "PicoScope 7 T&M Early Access" software, respectively. To calculate the impact velocity and contact time, the following steps were undertaken and repeated for each iteration- a total of three runs per sample volume.

1. The impact velocity, as briefly described in section 2.2, is measured using the photomicrosensors attached towards the bottom of the stopper stage with a gap of 2.00 cm. The photomicrosensors work based on slotted optical switches where status indication (on or off) is provided through the interruption of the infrared light within the phototransistors. The metal slice attached on the dropping platform, as seen in Fig. 11(b), passes through the photomicrosensors during the drop, interrupting the light beam and allowing the detection of the time taken for the dropping platform to travel over the 2.00 cm gap. The change in time is calculated using the graph of voltage against time provided from the PicoScope 7 T&M software as illustrated in Fig. 12.

The impact velocity, $\boldsymbol{v}$, was then calculated by taking the ratio of the distance travelled (2.00 cm) to the time taken, $\boldsymbol{\Delta t}$, using Eq. 1:

$$Impact\ velocity, v = \frac{Distance}{Time\ (\Delta t)} \quad (1)$$

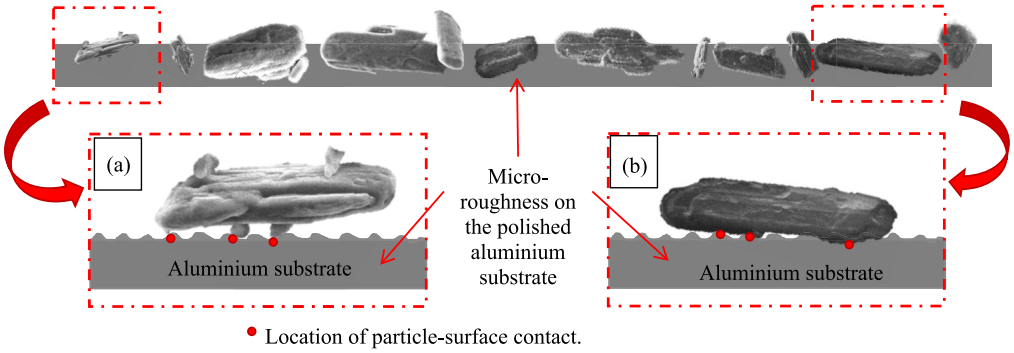


**Fig. 14.** Hypothetical schematic of variations in particle-surface contact area.

A total of 30 runs was undertaken to ensure the repeatability of the impact time using the drop test rig. For the drop height of 15 cm which was chosen for the experiments on ibuprofen powders, an average time of 12.99 ± 0.30 ms was taken for the dropping platform to travel between photomicrosensors with a gap of 2.00 cm. This generated an impact velocity of 1.54 ± 0.04 m/s, compared to the freefall velocity of 1.72 m/s (in vacuum) from 15 cm. For the aluminium-alloy powder, the drop height of 10 cm was used, which resulted into an average time of 16.23 ± 0.03 ms and a corresponding impact velocity of 1.23 ± 0.01 m/s.

.

2. The voltage generated by the piezoelectric ring during impact is used to calculate the contact time between the dropping platform and the stopper stage. As it can be seen in Fig. 13, the voltage starts to rise as the dropping platform touches the piezoelectric ring Fig. 11((c)) and reaches a peak when the dropping platform comes to the rest (corresponding to the peak impact force). The contact time during detachment is the time taken for the voltage to reach maximum.

To ensure the repeatability and accuracy of the contact time, a total of 30 runs was undertaken which resulted into an average contact time value of 81 ± 2 μs for a 15 cm drop and 83 ± 1 μs for a 10 cm drop.

3. The particle detachment force, $\boldsymbol{F_{det}}$, is then calculated by employing Newton's second law of motion expressed by Eq. 2, where $\boldsymbol{m}$ is the mass of the particle, $\boldsymbol{v}$ is the impact velocity calculated in step 1 and $\boldsymbol{\Delta t}$ is the contact time during detachment as calculated in step 2.

$$F_{det} = \frac{mv}{\Delta t} \tag{2}$$

When the adhesive forces, $\boldsymbol{F_{ad}}$, are greater than the detachment forces, $\boldsymbol{F_{det}}$, the particles will remain attached on the surface of the substrate but the contrary will occur when the detachment forces, $\boldsymbol{F_{det}}$ is greater than the adhesive forces, $\boldsymbol{F_{ad}}$ [30]. Therefore, for a given impact velocity, which is 1.54 m/s in this work, there is a critical particle diameter above which the particles will detach from the surface and below this size will remain attached after impact. Based on the JKR model of adhesion [12] the effective work of adhesion is then calculated for the particles by equating the adhesive force, $\boldsymbol{F_{ad}}$, to the detachment force, $\boldsymbol{F_{det}}$ by using Eqs. 3 and 4.

$$F_{ad} = \frac{3}{2}\pi R\Gamma \tag{3}$$

$$\frac{3}{2}\pi R\Gamma = \frac{mv}{\Delta t} \tag{4}$$

## 3. Results and discussion

### 3.1. The effect of quantity of sample on the manual isolation of critical diameter and effective work of adhesion

Determining the required volume of sample (in terms of number of particles) is paramount for accurately measuring the critical diameter at a given impact velocity. Due to the limited availability of API's in the early development stage, only a certain amount of material may be used, which poses restrictions on the bulk powder flow characterisation. However, it is important to establish a threshold in sample quantity and total particle number, below which the accuracy of results may be significantly compromised for a given material.

The critical diameter of the ibuprofen powders has been calculated at different sample volumes: 7 $mm^3$, 21 $mm^3$, 42 $mm^3$, and 49 $mm^3$ so as to obtain the minimum quantity required. The temperature and humidity were at ambient lab conditions ranging from 22.4 °C to 24.6 °C and 43 % to 54 %, respectively, while the drop height was maintained at 15 cm, which resulted into an impact velocity of 1.54 ± 0.04 m/s and a contact time of 81 ± 2 μs. The choice of the drop height at 15 cm was based on the adhesive properties of particles such that enough number of particles would remain attached to the substrate after the drop test for analysis.

According to Zafar et al. [30] particles above the critical diameter will detach from the substrate at a given impact velocity ($F_{det} > F_{ad}$), while particle below will remain attached ($F_{det} < F_{ad}$). This would suggest that the finer particles, below the critical diameter, will remain attached on the substrate while the larger particles will detach after impact. The reason for the finer particles still adhering on the substrate while the larger particles detach is due to the ratio of adhesion over gravitational forces (momentum). Furthermore, the Bond number (Bo) which is defined as the ratio of the particle adhesion force to the particle weight suggests that finer particles exhibit lower weights compared to larger particles, resulting into higher adhesion forces. The same observation was made by Salazar-Banda et al. [44] on their study of adhesion force between particles on a flat surface using the centrifuge method, where they stated that the ratio of van der Waals to gravitational forces was significantly higher in finer particles. Theoretically, smaller particles will remain attached on the substrate compared to the larger particles after impact as explained earlier. However, through the series of experiments undertaken in this work, it was observed (Supplementary Data, S1: Appendix A) that in majority of the cases, few smaller particles detached while some of the larger particles remained attached after the impact. This suggests the complexities associated with the contact area between the particle and substrate, particularly for irregularly shaped particles such as the ibuprofen powders used in this work. The irregular particle morphologies may result into variations in geometry/orientation and contact points with the aluminium substrate upon dispersion, which significantly influences the calculations for the effective work of

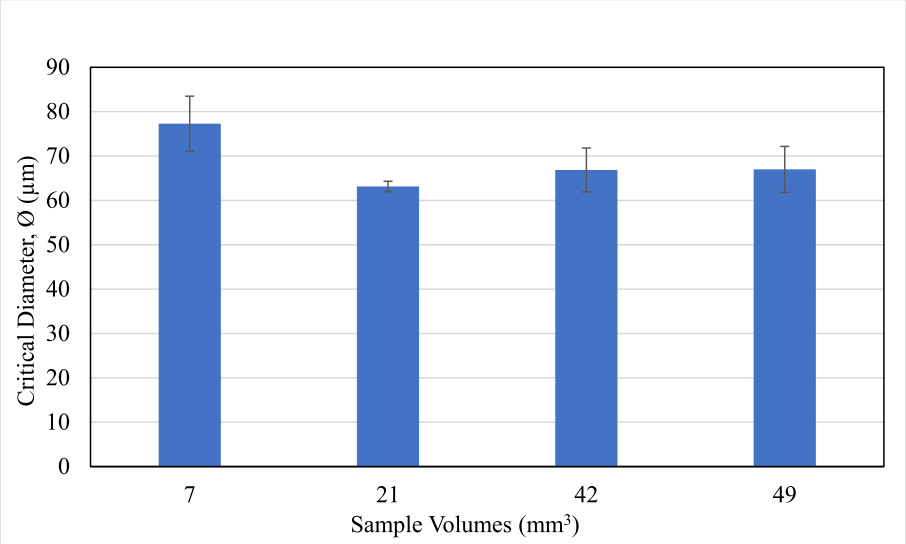


**Fig. 15.** Critical Diameter, Ø (μm) of ibuprofen powders dropped at 15 cm.

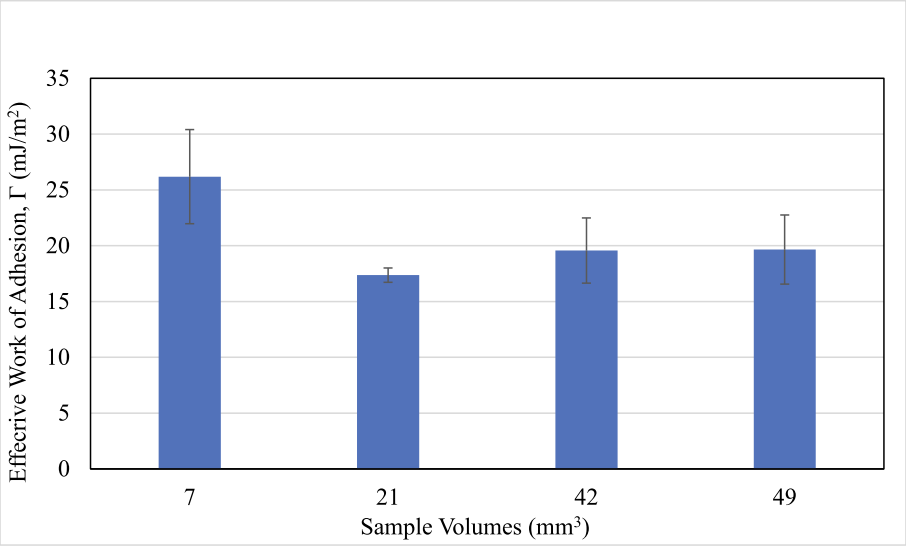


**Fig. 16.** Effective work of adhesion, Γ, (mJ/m$^2$) ibuprofen powders dropped at 15 cm.

adhesion. Additionally, the aluminium substrate may not be perfectly polished, which may result into micro-roughness on the surface of the substrate. Fig. 14 demonstrates that micro-roughness on both the polished substrate and particles may result into variations in the contact area and consequently affect the calculations of the effective work of adhesion. Fig. 14(a) illustrates a particle of a significantly smaller size compared to Fig. 14(b) which is a much larger particle, where the smaller particle detaches upon impact while the larger particle remains attached to the substrate. This suggests that the smaller particle established fewer contact points with the substrate compared to the larger particle. It is therefore imperative to establish a criterion for calculating the work of adhesion of irregularly shaped particles that possess significant variations in contact area. For this purpose, the critical diameter at a given impact velocity is believed to lie within the range of particles still adhered on the substrate after impact and the subsequent particles detached from the substrate. Hence, as described in section 2.4 (further details found in Supplementary Data, S1: Appendix A) the mean of the average mass per particle post-drop test and the average mass per detached particle is calculated. This value, which is known as the average critical mass per particle, $m_{avg,critical}$, is then converted into an equivalent critical diameter, $d_c$.

Fig. 15 shows that the obtained critical diameters are 77 ± 6 μm, 63 ± 1 μm, 67 ± 5 μm to 67 ± 5 μm for the ibuprofen sample volumes of 7 mm$^3$, 21 mm$^3$, 42 mm$^3$, and 49 mm$^3$, respectively. It is evident that there are no significant changes observed between the critical diameters obtained from the sample volumes of 42 mm$^3$ and 49 mm$^3$. This suggests that for optimisation purposes of the ibuprofen powder, a minimum quantity of 42 mm$^3$ is required to ensure the accurate measure of the critical diameter, with enough number of particles present for analysis. This is also evident in Fig. 16 where the effective work of adhesion, $\Gamma$ of ibuprofen particles ranged from 26.2 ± 4.2 mJ/m$^2$, 17.4 ± 0.6 mJ/m$^2$, 19.6 ± 2.9 mJ/m$^2$ to 19.7 ± 3.1 mJ/m$^2$ across the sample volumes reach a steady value above 42 mm$^3$.

Additionally, the total number of particles initially dispersed on the substrate was also calculated where an average of 239, 481, 644 and 926 particles where present for the sample volumes of 7 mm$^3$, 21 mm$^3$, 42 mm$^3$, and 49 mm$^3$, respectively. For the ibuprofen with the particle size distribution measured in Table 1 and Table 2, it can be suggested that a minimum number of approximately 644 particles is required to be dispersed on the substrate before the drop test to ensure the accuracy of

**Table 5**
Summary of the findings of the different sample volumes.

| Sample | Total number of particles dispersed | Critical, Ø (μm) | Detachment Force, $F_{det}$ (μN) | Effective Work of Adhesion, Γ (mJ/m$^2$) |
|---|---|---|---|---|
| Ibuprofen 7 mm$^3$ | 239 | 77 ± 6 | 4.8 ± 1.2 | 26.2 ± 4.2 |
| Ibuprofen 21 mm$^3$ | 481 | 63 ± 1 | 2.6 ± 0.1 | 17.4 ± 0.6 |
| Ibuprofen 42 mm$^3$ | 644 | 66 ± 5 | 3.1 ± 0.7 | 19.6 ± 2.9 |
| Ibuprofen 49 mm$^3$ | 926 | 67 ± 5 | 3.1 ± 0.8 | 19.7 ± 3.1 |

the calculations. Table 5 below provides a summary of the findings over the four sample volumes.

### 3.2. Automated measurement of the critical diameter and calculation of effective work of adhesion

For a more time efficient calculation of the critical diameter an automated image analysis algorithm was developed to determine the particle size distribution of the substrate. Manual calculation of the particle size distribution, post-dispersion and post-drop test proved to be time consuming, hence the automated methodology provided an efficient solution to this problem. Fig. 17 demonstrates the values of the critical diameter calculated from both the manual and automated methods. The critical diameters ranged from 80 ± 5 μm, 70 ± 3 μm, 70 ± 4 μm to 70 ± 3 μm for the sample volumes of 7 mm$^3$, 21 mm$^3$, 42 mm$^3$, and 49 mm$^3$, respectively. Generally, the critical diameters calculated from the manual and automated methodology lie within the same range except some discrepancies present in sample volume 21 mm$^3$. This is due to some limitations posed on the detection of the clusters and agglomerates, which can easily be observed and isolated manually but may not

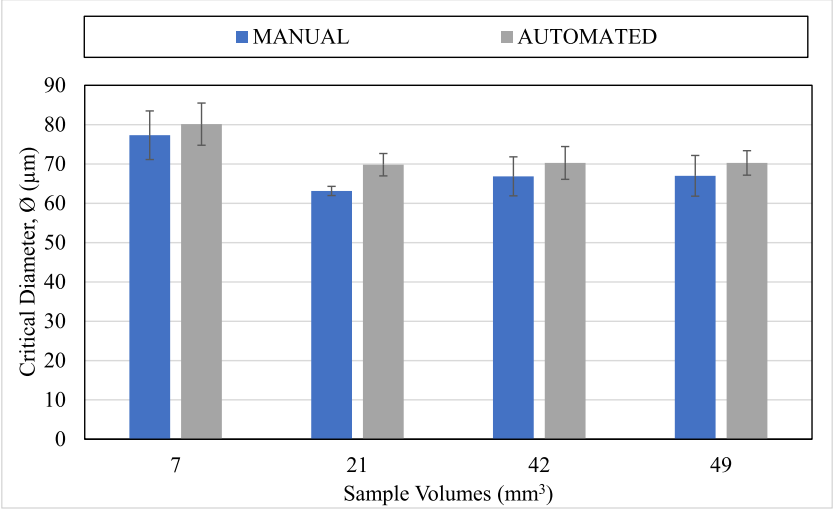


**Fig. 17.** Comparison between manual and automated critical diameter of ibuprofen powders over the four sample volumes.

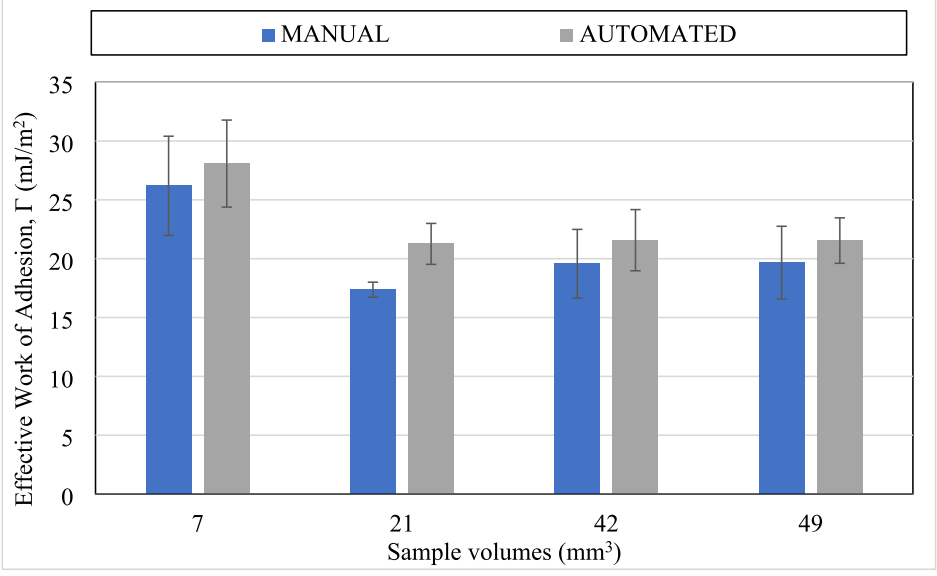


**Fig. 18.** Comparison between manual and automated effective work of adhesion of ibuprofen powders over the four sample volumes.

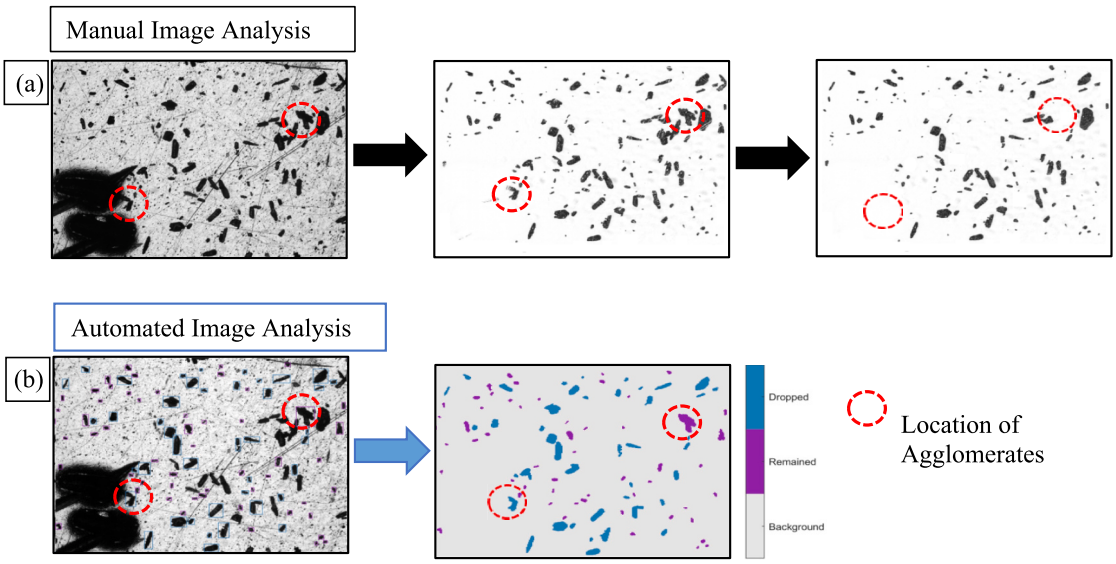


**Fig. 19.** (a) Manual image analysis and (b) automated image analysis. Note: the large black marks on the images are the reference points.

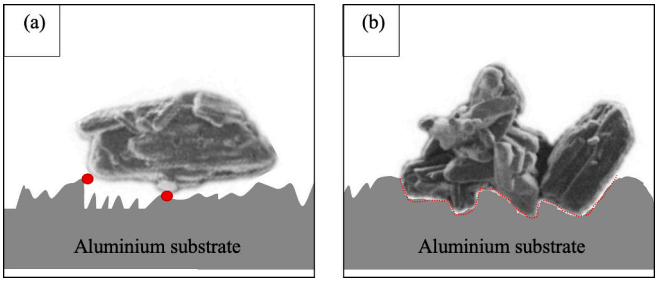


**Fig. 20.** Hypothetical illustration of an (a) Agglomerate that detaches after the drop test due to fewer particle to substrate contacts and (b) agglomerate that remains attached after the drop test due to sufficient particle-substrate contact.

be successfully detected automatically (Fig. 19).

Furthermore, the effective work of adhesion, $\Gamma$ across 7 $mm^3$, 21 $mm^3$, 42 $mm^3$, and 49 $mm^3$, was calculated and ranged from 28.1 ± 3.7 $mJ/m^2$, 21.3 ± 1.7 $mJ/m^2$, 21.6 ± 2.6 $mJ/m^2$ to 21.5 ± 1.9 $mJ/m^2$, respectively. Fig. 18 demonstrates that the values calculated from the manual and automated methodologies lie within the same range, which is promising for a more time effective analysis. As stated previously the discrepancies between the manual and automated values maybe due to the unsuccessful automatic detection of powder agglomerates and clusters. The automated exclusion of agglomerates may pose challenges as they can be subjective and tricky for particles that are far from spherical, either elongated or with rougher edges. It is evident from Fig. 19 that there are visible agglomerates on the substrate which are required to be removed for accurate isolation of single particles. Fig. 19 (a) illustrates that the agglomerates and clusters have manually been removed, however, this was not very successful in the automated isolation of single particles as portrayed in Fig. 19(b).

It is also important to note that the main source of error within these calculations arise from the mass of an individual particle. The analysis is based on calculating the effective work of adhesion of a single particle in contact with the substrate, hence taking into account agglomerates or clusters compromises the accuracy of the results. Theoretically, agglomerates tend to detach from the substrate after impact as they have

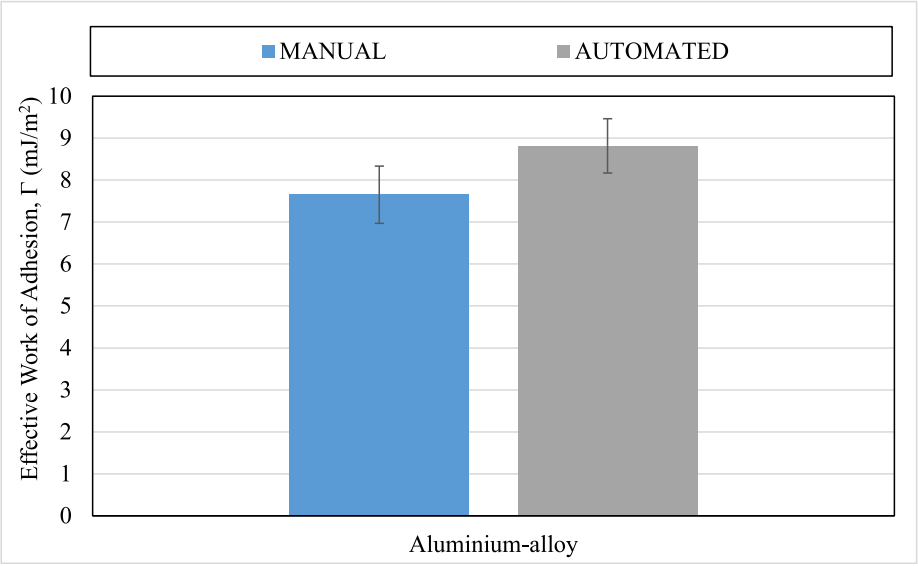


**Fig. 21.** Comparison between manual and automated calculated effective work of adhesion of spherical Aluminium-alloy metal powders.

larger masses, however in a few cases the agglomerates continued to adhere on the substrate after impact. This may be due to the difference in their contact area with the substrate as compared to equal sized single particles. Fig. 20 illustrates a hypothetical schematic of the complexities associated with particle-surface contact of agglomerates. It is important to note that the surface roughness of the substrates have been exaggerated to depict the variations of contact between the agglomerate and substrate. Fig. 20(a) depicts an agglomerate that detaches easily after the drop test due to fewer points of contact (red zones) while Fig. 20(b) shows an agglomerate that remains attached after impact due to its position on the substrate resulting into sufficient particle-wall contact (red zones). This further suggests the complexities associated with particle-wall interactions such as surface roughness on both the particles and the substrate.

Additionally, the experimental work was further extended to investigate the effective work of adhesion of spherical powders on the substrate. Aluminium-alloy metal powders were investigated using the exact same methodology but at a drop height of 10 cm. The drop height was changed due to the nature of the metal powder, where no particles adhered on the substrate after the drop test at drop heights greater than 10 cm. 7 $mm^3$ of powder was dispersed on top of the substrate which resulted into approximately 1340 particles across four iterations and a critical diameter of 40 ± 2 μm. Fig. 21 compares the manual and automated methods for evaluating the effective work of adhesion, $\Gamma$ of the spherical Aluminium-alloy metal powders. The effective work of adhesion, $\Gamma$ calculated was 7.7 ± 1.8 $mJ/m^2$ and 8.8 ± 1.6 $mJ/m^2$ using the manual and automated techniques, respectively. It is evident that the effective work of adhesion, $\Gamma$ for the spherical aluminium-alloy powders is significantly lower than the irregularly shaped ibuprofen powders. While the chemical nature of the two materials is different giving rise to a difference in their surface energies, the spherical powders establish fewer contact points with the substrate due to their regular and smoother morphologies, enabling them to easily detach after the drop test.

## 4. Conclusion

This study was aimed at measuring the effective work of adhesion of the irregularly shaped ibuprofen powders by defining a window of operation using the drop test method. This work was also extended to measuring the effective work of adhesion of spherically shaped aluminium-alloy powders. The further development of the drop test rig ensured more reliable and repeatable measurements of the impact velocity and contact time. A total of 30 iterations was undertaken to ensure the repeatability of the impact time, by releasing the dropping platform at a height of 15 cm (for ibuprofen powders), resulting into an impact velocity of 1.54 ± 0.04 m/s. The corresponding, contact time was measured 81 ± 2 μs. Additionally, a drop height of 10 cm was implemented for the spherical aluminium-alloy metal powders as any height above this resulted to no particles remaining adhered on the substrate after the drop test. The 10 cm drop height resulted into an impact velocity of 1.23 ± 0.01 m/s and a contact time of 83 ± 1 μs.

Furthermore, the incorporation of the automated image analysis for the detection of the critical diameter, above which particles detach from the substrate and below which powders adhere onto the surface, has provided an accurate and efficient solution to the manual image analysis. The findings in this study suggests that a minimum quantity of sample is required to be dispersed on the substrate so as to ensure accuracy of measurements. For the ibuprofen powders, with a particle size distribution summarised in Table 1, it can be deduced that 644 particles need to be dispersed on the substrate to accurately calculate the effective work of adhesion. This suggests a threshold in the number of particles required for the initial dispersion, below which the accuracy of results is significantly compromised. The effective work of adhesion of 19.6 ± 2.9 $mJ/m^2$ was measured for the ibuprofen powders at an impact velocity of 1.54 ± 0.04 m/s. Additionally, the effective work of adhesion of spherical aluminium-alloy metal powders was also measured at 7.7 ± 1.8 $mJ/m^2$ and 8.8 ± 1.6 $mJ/m^2$ using the manual and automated techniques, respectively. This work provides a feasible solution for calculating the work of adhesion between particle-surface contact at a time and cost-effective manner with the integration of an automated image analysis. It is important to note that the minimal threshold established for a sample is dependant to the particle size distribution. Hence, for any given sample, a threshold for the number of particles initially dispersed on the substrate needs to be established to ensure the accuracy of results. Furthermore, the choice for the drop height is also material dependant so as to ensure that there are particles still adhered on the substrate after the drop test to enable analysis.

## CRediT authorship contribution statement

**Fatemeh A. Talebi:** Writing – original draft, Methodology, Investigation, Formal analysis, Data curation, Conceptualization. **Arash Rabbani:** Writing – review & editing, Supervision, Methodology, Investigation, Formal analysis, Data curation, Conceptualization. **Mozhdeh Mehrabi:** Writing – review & editing, Supervision, Methodology, Investigation, Conceptualization. **Andrew Stockdale:** Methodology, Writing – review & editing. **David Harbottle:** Writing – review & editing, Supervision, Investigation, Conceptualization. **Mehrdad Pasha:** Visualization, Conceptualization. **Ali Hassanpour:** Writing – review & editing, Visualization, Supervision, Methodology, Investigation, Formal analysis, Conceptualization.

## Declaration of competing interest

The authors declare that they have no known competing financial interests or personal relationships that could have appeared to influence the work reported in this paper.

## Acknowledgement

The authors acknowledge the technical support provided Matthew Buckley for implementing the electrical elements on the drop test rig. The authors would also like to thank Professor Mojtaba Ghadiri and his research group for facilitating access to the Morphologi G3® which was integral to this study. We also acknowledge the technical support provided by Dr. Ben Douglas from School of Chemical and Process Engineering, Ms. Camille Hammersley from the Institute of Functional Surfaces (IFS) - School of Mechanical Engineering, Dr. Mohamed Edokali, Dr. Jabbar Gardy and Mr. Stuart Micklethwaite (Leeds Electron microscopy and spectroscopy centre, LEMAS).

## Appendix A. Supplementary data

Supplementary data to this article can be found online at https://doi.org/10.1016/j.powtec.2024.120605.

## Data availability

Data will be made available on request.

## References

[1] J.K. Prescott, R.A. Barnum, On powder flowability, Pharm. Technol. 24 (10) (2000) 60–82.
[2] M. Capece, R. Ho, J. Strong, P. Gao, Prediction of powder flow performance using a multi-component granular bond number, Powder Technol. 286 (2015) 561–571.
[3] F.J. Muzzio, T. Shinbrot, B.J. Glasser, Powder Technology in the Pharmaceutical Industry: the Need to Catch Up Fast vol. 124, 2002, pp. 1–7, ed: Elsevier.
[4] Y. Qiu, Y. Chen, G.G. Zhang, L. Yu, R.V. Mantri, Developing Solid Oral Dosage Forms: Pharmaceutical Theory and Practice, Academic press, 2016.
[5] S. Bibiceva, S.L.M. Schroeder, A. Hassanpour, Auto-agglomeration of dry ibuprofen powder under mechanical vibration: effect of particle morphology and surface

properties, Powder Technol. 433 (2024) 119172, 2024/01/15/, https://doi.org/10.1016/j.powtec.2023.119172.
[6] L.X. Liu, I. Marziano, A.C. Bentham, J.D. Litster, E.T. White, T. Howes, Effect of particle properties on the flowability of ibuprofen powders, Int. J. Pharm. 362 (1) (2008) 109–117, 2008/10/01/, https://doi.org/10.1016/j.ijpharm.2008.06.023.
[7] X. Han, C. Ghoroi, D. To, Y. Chen, R. Davé, Simultaneous micronization and surface modification for improvement of flow and dissolution of drug particles, Int. J. Pharm. 415 (1) (2011) 185–195, 2011/08/30/, https://doi.org/10.1016/j.ijpharm.2011.05.070.
[8] M.E. Aulton, K. Taylor, Aulton's Pharmaceutics: The Design and Manufacture of Medicines, Elsevier Health Sciences, 2013.
[9] M.S. Escotet-Espinoza, et al., Improving feedability of highly adhesive active pharmaceutical ingredients by silication, J. Pharm. Innov. 16 (2021) 279–292.
[10] H.-J. Butt, M. Makowski, M. Kappl, A. Ptak, On the adhesion between individual particles, Kona Powder Part. J. 29 (2011) 53–66.
[11] W. Nan, et al., Jamming during particle spreading in additive manufacturing, Powder Technol. 338 (2018) 253–262, 2018/10/01/, https://doi.org/10.1016/j.powtec.2018.07.030.
[12] K.L. Johnson, K. Kendall, A. Roberts, Surface energy and the contact of elastic solids, Proc. Royal Soc. London. A. Math. Phys. Sci. 324 (1558) (1971) 301–313.
[13] S. Chen, W. Liu, S. Li, A fast adhesive discrete element method for random packings of fine particles, Chem. Eng. Sci. 193 (2019) 336–345, 2019/01/16/, https://doi.org/10.1016/j.ces.2018.09.026.
[14] C. Windows-Yule, A. Neveu, Calibration of DEM simulations for dynamic particulate systems, Pap. Phys. 14 (2022) 140010.
[15] J.J. Wang, T. Li, S.D. Bateman, R. Erck, K.R. Morris, Modeling of adhesion in tablet compression—I. Atomic force microscopy and molecular simulation, J. Pharm. Sci. 92 (4) (2003) 798–814.
[16] D. Freiberg, A. Zavaliangos, Adhesion of powder onto tools during compaction: a numerical study, Powder Technol. 407 (2022) 117644, 2022/07/01/, https://doi.org/10.1016/j.powtec.2022.117644.
[17] R. Mukherjee, C. Mao, S. Chattoraj, B. Chaudhuri, DEM based computational model to predict moisture induced cohesion in pharmaceutical powders, Int. J. Pharm. 536 (1) (2018) 301–309, 2018/01/30/, https://doi.org/10.1016/j.ijpharm.2017.12.001.
[18] P. Petean, M. Aguiar, Determining the adhesion force between particles and rough surfaces, Powder Technol. 274 (2015) 67–76.
[19] A.D. Zimon, Adhesion of Dust and Powder, Springer Science & Business Media, 2012.
[20] D.T. Tran, R. Bittner, P. Zámostný, Adhesion force measurement by centrifuge technique as tool for predicting interactive mixture stability, Chem. Eng. Res. Des. 165 (2021) 467–476.
[21] M. Davies, et al., Characterization of drug particle surface energetics and Young's modulus by atomic force microscopy and inverse gas chromatography, Pharm. Res. 22 (2005) 1158–1166.
[22] Y. Shimada, M. Tsubota, S. Matsusaka, Measurement of particle adhesion force and effective contact radius via centrifuge equipped with horizontal and vertical substrates, Powder Technol. 397 (2022) 117103.
[23] K. Higashitani, H. Makino, S. Matsusaka, Powder Technology Handbook, CRC Press, 2019.
[24] Z. Zhang, M.A. Ferenczi, C.R. Thomas, A micromanipulation technique with a theoretical cell model for determining mechanical properties of single mammalian cells, Chem. Eng. Sci. 47 (6) (1992) 1347–1354, 1992/01/01/, https://doi.org/10.1016/0009-2509(92)80280-P.
[25] M.J. Chen, Z. Zhang, T.R. Bott, Direct measurement of the adhesive strength of biofilms in pipes by micromanipulation, Biotechnol. Tech. 12 (12) (1998) 875–880, 1998/12/01, https://doi.org/10.1023/A:1008805326385.
[26] S. Hu, T.-H. Kim, J.-G. Park, A.A. Busnaina, Effect of different deposition mediums on the adhesion and removal of particles, J. Electrochem. Soc. 157 (6) (2010) H662.
[27] P. Kulkarni, P.A. Baron, K. Willeke, Aerosol measurement: principles, techniques, and applications, John Wiley & Sons, 2011.
[28] T. Deng, V. Garg, M.S.A. Bradley, A study of particle adhesion for cohesive powders using a novel mechanical surface energy tester, Powder Technol. 391 (2021) 46–56, 2021/10/01/, https://doi.org/10.1016/j.powtec.2021.06.002.
[29] E. Ermis, R.J. Farnish, R.J. Berry, M.S.A. Bradley, Centrifugal tester versus a novel design to measure particle adhesion strength and investigation of effect of physical characteristics (size, shape, density) of food particles on food surfaces, J. Food Eng. 104 (4) (2011) 518–524, 2011/06/01/, https://doi.org/10.1016/j.jfoodeng.2011.01.008.
[30] U. Zafar, C. Hare, A. Hassanpour, M. Ghadiri, Drop test: a new method to measure the particle adhesion force, Powder Technol. 264 (2014) 236–241.
[31] L. Pedrolli, S. Nadimi, B. Achiaga, A. López, Estimation of mesoscale surface energy in the kinetic adhesion test, Powder Technol. 435 (2024) 119426, 2024/02/15/, https://doi.org/10.1016/j.powtec.2024.119426.
[32] L. Pedrolli, S. Nadimi, S. Maramizonouz, B. Achiaga Menor, A. López, Kinetic adhesion test to determine particle surface energy, HardwareX 14 (2023), https://doi.org/10.1016/j.ohx.2023.e00437.
[33] M. G3 and U. Manual, "Malvern instruments ltd," United Kingdom, Man0410, 2008 [Online]. Available: https://www.federation-fermat.fr/wp-content/uploads/2019/09/Morphologi_G3_User-Manual_MAN0410-1.1_0.pdf.
[34] G.B. Basim, M. Khalili, Particle size analysis on wide size distribution powders; effect of sampling and characterization technique, Adv. Powder Technol. 26 (1) (2015) 200–207, 2015/01/01/, https://doi.org/10.1016/j.apt.2014.09.009.
[35] J. Schindelin, et al., Fiji: an open-source platform for biological-image analysis, Nat. Methods 9 (7) (2012) 676–682, 2012/07/01, https://doi.org/10.1038/nmeth.2019.
[36] G.R. Terrell, D.W. Scott, Oversmoothed nonparametric density estimates, J. Am. Stat. Assoc. 80 (389) (1985) 209–214, 1985/03/01, https://doi.org/10.1080/01621459.1985.10477163.
[37] M. Styner, C. Brechbuhler, G. Szckely, G. Gerig, Parametric estimate of intensity inhomogeneities applied to MRI, IEEE Trans. Med. Imaging 19 (3) (2000) 153–165.
[38] H.-G. Beyer, H.-P. Schwefel, Evolution strategies–a comprehensive introduction, Nat. Comput. 1 (2002) 3–52.
[39] A. Rabbani, M. Babaei, Hybrid pore-network and lattice-Boltzmann permeability modelling accelerated by machine learning, Adv. Water Resour. 126 (2019) 116–128.
[40] R. Fabbri, L.D.F. Costa, J.C. Torelli, O.M. Bruno, 2D Euclidean distance transform algorithms: a comparative survey, ACM Comp. Surveys (CSUR) 40 (1) (2008) 1–44.
[41] G. Fu, S.A. Hojjat, A.C. Colchester, Integrating watersheds and critical point analysis for object detection in discrete 2D images, Med. Image Anal. 8 (3) (2004) 177–185.
[42] F. Meyer, Topographic distance and watershed lines, Signal Process. 38 (1) (1994) 113–125.
[43] T.G. Baychev, et al., Reliability of algorithms interpreting topological and geometric properties of porous media for pore network modelling, Transp. Porous Media 128 (2019) 271–301.
[44] G.R. Salazar-Banda, M.A. Felicetti, J.A.S. Gonçalves, J.R. Coury, M.L. Aguiar, Determination of the adhesion force between particles and a flat surface, using the centrifuge technique, Powder Technol. 173 (2) (2007) 107–117, 2007/04/19/, https://doi.org/10.1016/j.powtec.2006.12.011.